A Study on Function-Expansion-Based Topology Optimization without Gray Area for Optimal Design of Photonic Devices

| PAPER | *Special Section on Recent Advances in Simulation Techniques and Their Applications for Electronics* |

A Study on Function-Expansion-Based Topology Optimization without Gray Area for Optimal Design of Photonic Devices

Masato TOMIYASU[†a)], **Keita MORIMOTO**[†b)], *Student Members*, **Akito IGUCHI**[†c)], *Member*, *and* **Yasuhide TSUJI**[†d)], *Senior Member*

SUMMARY In this paper, we reformulate a sensitivity analysis method for function-expansion-based topology optimization method without using gray area. In the conventional approach based on function expansion method, permittivity distribution contains gray materials, which are intermediate materials between core and cladding ones, so as to let the permittivity differentiable with respect to design variables. Since this approach using gray area dose not express material boundary exactly, it is not desirable to apply this approach to design problems of strongly guiding waveguide devices, especially for plasmonic waveguides. In this study, we present function-expansion-method-based topology optimization without gray area. In this approach, use of gray area can be avoided by replacing the area integral of the derivative of the matrix with the line integral taking into account the rate of boundary deviation with respect to design variables. We verify the validity of our approach through applying it to design problems of a T-branching power splitter and a mode order converter.

key words: topology optimization, function expansion method, finite element method, adjoint variable method

1. Introduction

In order to develop high performance photonic devices beyond human knowledge, development of automatic optimization methods with high design flexibility is desired [1]–[18]. For this purpose, topology optimization methods which can optimize material distribution itself have been intensively studied to enhance performance of photonic devices. Several design approaches based on toptology optimization have already been reported and developed so far [5]–[18]. In topology optimization, optimization problem of material distribution itself is replaced with minimization or maximization problem of a specific objective function. To solve the problem, gradient-based methods based on sensitivity analysis or evolutionary methods have been employed. Topology optimization based on sensitivity analysis require iterative calculation of numerical simulation and estimation of sensitivity, which is variation of device performance with respect to design variables. Evolutionary approaches based on multiple point search can search wider range of searching space, but it cost a numerous computational effort. Since a vast number of design variables has to

be optimized, gradient-based approach is widely employed in topology optimization. As a representation method of material distribution, a function-expansion-method [9]–[14] is employed, and it has a feature that complexity of device profile can be adjusted by controlling number of function expansion terms. In the function-expansion-based topology optimization based on sensitivity analysis, material distribution contains gray materials, which are intermediate materials between core and cladding ones, during optimization procedure in order to let permittivity distribution differentiable and to compute sensitivity. However, use of gray area is not desirable in design of strongly guiding devices because this approach can not express material boundary exactly. In this paper, we revise the function-expansion-based topology optimization so as not to require gray area both in the waveguide analysis and the sensitivity analysis. In our approach, the sensitivity is estimated without gray materials by computing variation of permittivity at material boundary. The finite element method (FEM) is employed to analyze transmission property of optical devices. Although we have developed the automatic finite element mesh generation method for the function expansion method in [13], [14], flat triangular elements which degrade numerical accuracy might be generated. In this paper, we revise a finite element mesh generation method to improve finite element mesh.

In Sect. 2, the function-expansion-based topology optimization is briefly reviewed and the improved sensitivity analysis method is described. In addition, the improved adaptive mesh generation for function expansion method is illustrated. In Sect. 3, optimal design examples are shown and compared with those by the conventional approach to verify the validity of the present approach. Finally, this paper is concluded in Sect. 4.

2. Function Expansion Based Topology Optimization

2.1 Representation of Refractive Index Distribution

We consider an optimal design problem of photonic device with the desired transmission property, as shown in Fig. 1. In order to obtain optimal device structure, we employ the function expansion method to represent a structure in the design region and optimize the design variables by a gradient method according to the sensitivity analysis utilizing the adjoint variable method(AVM). In the function expansion method, the permittivity distribution is expressed as fol-
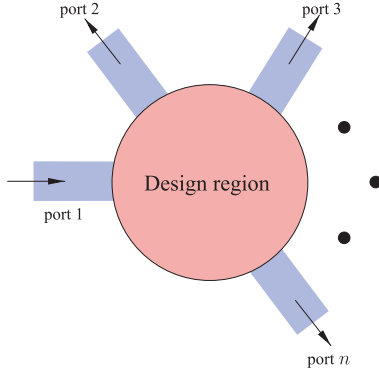
Fig. 1   Setup of design problem.

lows [9]:

$$\varepsilon_r(x,y) = \varepsilon_{ra} + (\varepsilon_{rb} - \varepsilon_{ra})H(w(x,y)) \tag{1}$$

$$w(x,y) = \sum_{i=1}^{N} c_i f_i(x,y) \tag{2}$$

where $w(x,y)$ is a structure expressing function given by the weighted sum of basis functions, $f_i(x,y)$. The amplitudes c_i of these basis functions are design variables in our design approach. Selection of basis functions is not unique and three kinds of functions have been compared in our previous work [12]. In this paper, we employ Fourier series which can dramatically change topology of device structure during an optimization process and the actual form will be shown in design examples. In the conventional function expansion method [9], $H(\xi)$ has been defined as a modified Heaviside function with continuous transition region from 0 to 1 as follows:

$$H(\xi) = \begin{cases} 0 & (\xi \leq -h) \\ \dfrac{1}{2}\left(\dfrac{\xi+h}{h}\right)^2 & (-h < \xi < 0) \\ 1 - \dfrac{1}{2}\left(\dfrac{\xi-h}{h}\right)^2 & (0 \leq \xi < h) \\ 1 & (\xi \geq h) \end{cases} \tag{3}$$

because of a requirement of permittivity function to be differentiable. However, an existing of gray areas in numerical modeling may degrade a numerical accuracy, especially in the design of plasmonic devices [13]. In this paper, $H(\xi)$ is defined as the original Heaviside function as follows:

$$H(\xi) = \begin{cases} 0 & (\xi < 0) \\ 1 & (\xi \geq 0) \end{cases} \tag{4}$$

and the sensitivity analysis method will be revised in the next subsection.

In the conventional sensitivity analysis based on the AVM, the gray area is required to take derivative of permittivity with respect to the design variables. The gray area is not desirable in design problems of strongly guiding photonic devices, especially for plasmonic devices. In this paper, we define $H(\xi)$ as Heaviside step function and revise

the sensitivity analysis method based on the AVM not to use gray area.

2.2   Sensitivity Analysis by Adjoint Variable Method

From Maxwell's equations, light propagation behavior is governed by the following wave equation:

$$\frac{\partial}{\partial x}\left(p\frac{\partial \phi}{\partial x}\right) + \frac{\partial}{\partial y}\left(p\frac{\partial \phi}{\partial y}\right) + k_0^2 q\phi = 0 \tag{5}$$

where p, q, ϕ are given for TE wave and TM waves as follows:

$$\begin{array}{llll} p = 1 & q = n^2 & \phi = E_z & \text{for TE wave} \\ p = \dfrac{1}{n^2} & q = 1 & \phi = H_z & \text{for TM wave} \end{array}$$

where $n = \sqrt{\varepsilon_r}$ is a refractive index distribution, and E_z and H_z are an z-component of electric and magnetic fields, respectively. In the FEM analysis, a final equation to be solved is given as a following simultaneous linear equation [19]:

$$[P(\varepsilon_r)]\{\phi\} = \{u\} \tag{6}$$

where $[P(\varepsilon_r)]$ is a finite element matrix, $\{\phi\}$ is an unknown nodal electric or magnetic field vector and $\{u\}$ is a vector related to an incident wave. In order to optimize design variables, we have to compute sensitivities of the transmission properties with respect to the design variables. Transmission power can be estimated using S-parameter. In the AVM, the sensitivity of S-parameter is expressed as follows [7]:

$$\frac{\partial S_{n1}}{\partial c_i} = -\{\lambda_n\}^T \frac{\partial [P(\varepsilon_r)]}{\partial c_i}\{\phi\}, \tag{7}$$

$$[P(\varepsilon_r)]^T \{\lambda_n\} = \{g_n\} \tag{8}$$

where $\{g_n\}$ is a vector related to the modal field in the n-th output port and $\{\lambda_n\}$ is an adjoint variable vector. In the conventional approach based on function expansion method, the derivatives of the matrix $[P]$ with respect to the design variables can be analytically obtained because ε_r is differentiable. In the conventional approach [7], $\partial[P]/\partial c_i$ is given as follows:

$$\frac{\partial [P]}{\partial c_i} = \sum_e \iint_e \frac{\partial \varepsilon_r}{\partial c_i}\frac{\partial [p(\varepsilon_r)]}{\partial \varepsilon_r} dxdy \tag{9}$$

$$\frac{\partial \varepsilon_r}{\partial c_i} = (\varepsilon_{rb} - \varepsilon_{ra})f_i(x,y) \left.\frac{\partial H(\xi)}{\partial \xi}\right|_{\xi=w(x,y)} \tag{10}$$

where $[p(\varepsilon_r)]_e$ is an integrand element matrix for matrix $[P(\varepsilon_r)]$ and $\sum_e$ extends over all elements in the design region.

In this paper, we define ε_r as a step profile at the material boundaries in order to eliminate gray area completely in the whole optimization process and the light propagation analysis. We revise the estimation of $\partial[P]/\partial c_i$ in (7) as follows:

$$\frac{\partial [P]}{\partial c_i} = \sum_e{}' \int_\Gamma \frac{\partial \delta}{\partial c_i}\left([p(\varepsilon_r^+)]_e - [p(\varepsilon_r^-)]_e\right) dl \tag{11}$$
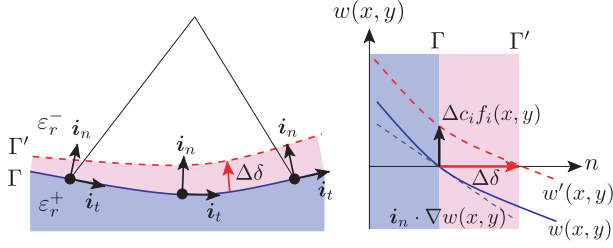
Fig. 2 Deviation of material boundary $\Delta\delta$ with respect to a slight change of design variable, Δc_i. Left figure is shown in xy-plane. Γ is material boundary and Γ' is a deviated material boundary. Right figure shows the relation between Δc_i and $\Delta\delta$.

Fig. 3 Improved finite element mesh generation scheme for function expansion method. (a) Finite element mesh by the scheme in [14]. (b) Structure expressed by function expansion method. (c) Generated boundary nodes on regular mesh. (d) Uniformly generated boundary nodes. (e) Generated inner nodes and generated mesh by Delauny triangulation. (f) Finally obtained mesh for second-order FEM analysis.

where $\sum'_e$ extends over all elements related to material boundary Γ, ε_r^+ and ε_r^- are the relative permittivity of the material on the right and left sides of the integration path, and $\partial\delta/\partial c_i$ denotes a deviation rate of Γ with respect to the design variable as shown in Fig. 2. This deviation rate is calculated as follows:

$$\frac{\partial\delta}{\partial c_i} = -\frac{f_i(x,y)}{i_n \cdot \nabla w(x,y)} \tag{12}$$

where i_n is a unit vector normal to Γ and δ is a function that changes along a material boundary.

2.3 Gradient Descent Method to Update Design Variables

We employ gradient descent method(GDM) to optimize design variables and update them as follows:

$$c_{\text{post}} = c_{\text{pre}} + \alpha \times (-\nabla_c C) \tag{13}$$

where c_{pre}, c_{post} are vectors consist of all the design variables before and after an update, respectively. $\nabla_c C$ express the gradient of the objective function C with respect to the design variables. α is defined as follows:

$$\alpha = \delta \times \frac{|C - C_{\text{opt}}|}{|\nabla_c C|} \tag{14}$$

where C_{opt} is the ideal value of the objective function and δ is a constant which governs a convergence speed in GDM. When α is larger, the property improvement may faster, however, the solution may oscillate around the optimal solution. By making α proportional to $|C - C_{\text{opt}}|$, The solution approaches the optimal solution faster when it is far from the optimal solution, and its neighborhood is searched in detail when it is close to the optimal solution. $\delta = 1.0$ is used in this paper.

2.4 Adaptive Finite Mesh Generation for Function Expansion Method

In the conventional function expansion method, it is not so important to treat material boundaries strictly because a permittivity distribution is defined as a continuous function. Since the sensitivies are estimated only at the material boundaries in the present approach, it is necessary to
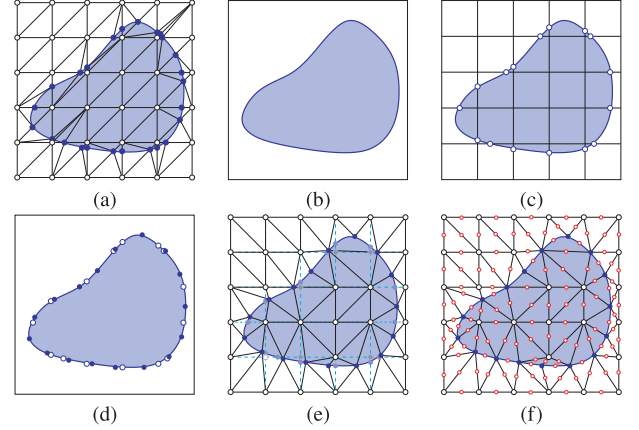
treat the boundaries strictly in order to calculate the sensitivity with good accuracy. We have presented the automatic finite element mesh generation for the function expansion method in [14]. However, the approach in [14] is not necessarily sufficient to calculate the sensitivity because there is a possibility that small elements or flattened elements are generated around the material boundary shown in Fig. 3(a) and cause degradation of accuracy for sensitivity evaluation. In this section, the mesh generation scheme is also improved so as to generate better elements around material boundaries.

The schematic of a finite element mesh generation is shown in Fig. 3. First, the material boundary is recognized on a regular lattice meshes and the crossing points of the regular mesh and material boundary are detected and stored (Fig. 3(c)). At this stage in Fig. 3(c), each distances between the neighboring nodes are not uniform, then the new nodes are placed uniformly on the material boundary (Fig. 3(d)), and all the nodes stored previously are removed. After that, the other nodes in the design region expect for near the material boundary (Fig. 3(e)), then finite element mesh is generated by a Delaunay triangulation and nodes for higher-order curvilinear elements are generated (Fig. 3(f)). Here, the nodes put on material boundary are not always on the material boundary exactly because at this point the linear approximation is used to find the material boundary. To express curved boundary more exactly, the nodes are moved on the boundary estimated by a Newton's method because $w(x,y)$ is a nonlinear function. The Newton's method is expressed as follows:

$$r' = r - \frac{w(r)}{i_n \cdot \nabla w(r)} \cdot i_n \tag{15}$$

where r is a initial position vector and r' is a corrected one by Newton's method. After an initial position of node is estimated by linear interpolation, this correction is iterated several times.
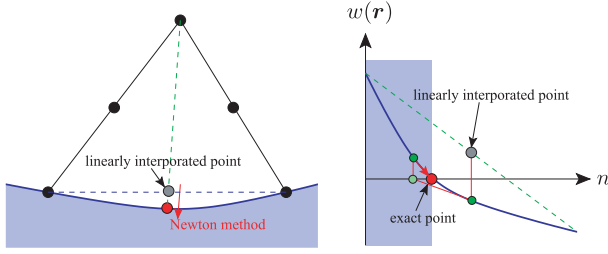
Fig. 4 An image to allocate node related to material boundary. A position of node is first set by linear interpolation and is moved onto material boundary by Newton's method.

3. Design Examples by the Proposed Method

In order to verify the validity of the present approach, first, we consider the design example of a T-branching waveguide [7] as shown in Fig. 5. The refractive indices of core and cladding materials are $n_1 = 1.45$ and $n_2 = 1$, respectively. The waveguide width is $w = 0.7 \ \mu$m, the design region width in the x and y directions are $W_x = 4 \ \mu$m and $W_y = 3 \ \mu$m, and $d = 1.5 \ \mu$m. The fundamental TE wave(TE$_0$) with the wavelength of $1.55 \ \mu$m is launched into port 1. In order to split the incident power equally between port 2 and 3, the objective function is given as follows:

$$\text{Minimize } C = \left|0.5 - |S_{21}|^2\right|^2 + \left|0.5 - |S_{31}|^2\right|^2. \quad (16)$$

In order to express device structure in the design region, we employ Fourier series as $w(x, y)$ in (2) as follows [7]:

$$w(x, y) = \sum_{j=0}^{N_y-1} \sum_{i=-N_x}^{N_x-1} (a_{ij} \cos \theta_{ij} + b_{ij} \sin \theta_{ij}) \quad (17)$$

$$\theta_{ij} = \frac{2\pi i}{L_x} + \frac{2\pi j}{L_y}$$

where a_{ij}, b_{ij} are design variables, and L_x, L_y are basic cycles of fourier series. We set $2N_x \times N_y = 16 \times 8$, $L_x = 1.2W_x$, and $L_y = 1.2W_y$ in this design example. Figure 6 shows the results obtained by the conventional optimization approach based on (9) with gray area [7] and the present one based on (11) without gray area. In this design example, the convergence behaviors of the objective functions and the finally obtained results are almost same. The normalized transmitted powers into port 2 and 3 are 0.46. Compared with the results reported previously in [7], the normalized transmitted powers are almost same while the obtained optimized structures are different. This is because there are many local optimal structures and optimized structure depends on an initial structure and optimization settings. An enlarged views of gray area in both results are shown in Fig. 6. Although gray area seems to be negligible compared with the entire design area, in the design of plasmonic devices, a transmission property may significantly change due to an existence of gray area [14].

As a second design example, we consider a mode converter that converts TE$_0$ wave into the first higher order TE
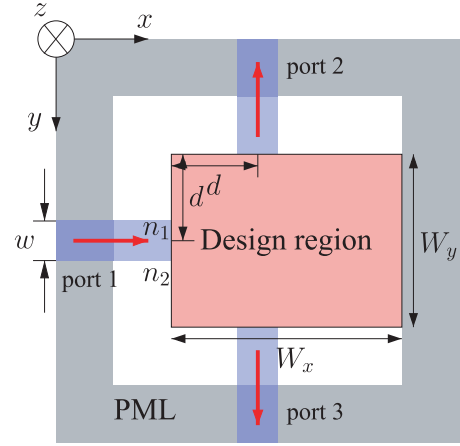

Fig. 5 Design model of two-branch.
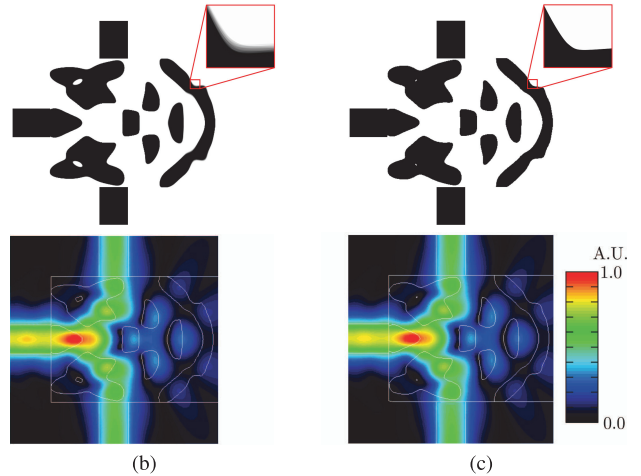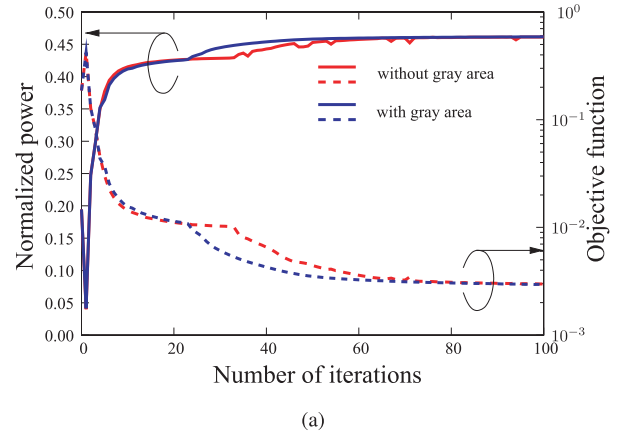

(a)

(b)   (c)

Fig. 6 Optimized results of T-branching waveguide. (a) The objective function and the normalized output power as a function of iteration count for topology optimization. The optimized structure and the propagating electric field obtained (b) with using gray area, (c) without using gray area.

wave (TE$_1$), as shown in Fig. 7. The refractive indices of core and cladding materials are $n_1 = 3.4$ and $n_2 = 1$, respectively. The waveguide width is $w = 0.45 \ \mu$m, the design region widths in the x and y directions are $W_x = 1 \ \mu$m and
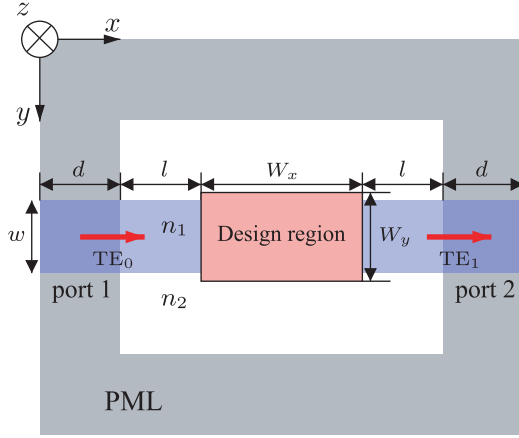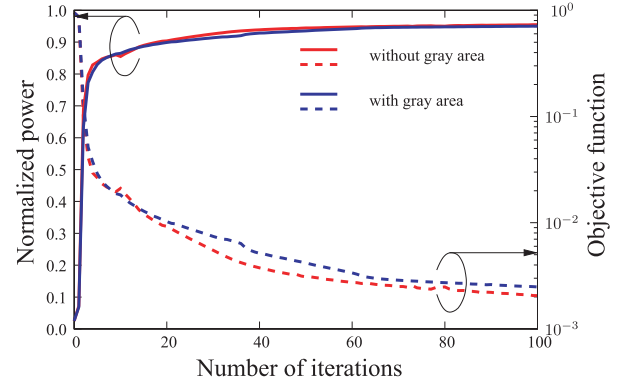
Fig. 7   Design model of mode order converter.

$W_y = 0.55 \ \mu$m, and $l = d = 0.5 \ \mu$m. TE_0 wave with the wavelength of 1.55 μm is launched into port 1. The objective function is given as follows:

$$\text{Minimize } C = \left| 1 - \left| S_{21}^{TE_0 \rightarrow TE_1} \right|^2 \right|^2. \qquad (18)$$

Fourier series with $2N_x \times N_y = 16 \times 8$ sampling points, $L_x = 1.2 W_x$, and $L_y = 1.2 W_y$ is used to construct $w(x, y)$. Figure 8 shows the results obtained by the conventional optimization approach using gray area and the present one without using gray area. Although the convergence behaviors of the objective functions and the finally obtained results are slightly different, the optimized devices have similar profile and almost the same performance. The conversion efficiencies (TE_0 to TE_1) is 0.954 in the optimized structure obtained by the present approach and 0.950 in that by the conventional approach. In Fig. 8, the structural evolution in the first 4 iteration steps are shown. Although the sensitivity is calculated only at the material boundary in the present optimization approach without gray area, the internal structure is updated and the topology of the structure automatically changes. This is due to the use of Fourier series as a structure expressing function. Tuning of a certain Fourier coefficient causes structural change over the entire design region because Fourier series is a basis function spreading throughout the design region. Therefore, there is the whole structure changes only by updating the material boundary.

Next, we investigate the influence of the device length, W_x, on the optimization results. Figure 9(a) shows the conversion efficiency of the optimized structure as a function of W_x. As shown in the figure, the conversion efficiency is improved as the device length increases. It can be seen that the conversion efficiency is hardly improved when the device length exceeds 1 μm. This is because the global optimal solution could not be found. This tendency is almost same in the conventional approach using gray area. The optimized structure with $W_x = 0.5 \ \mu$m and 1.5 μm and their propagating fields are shown in Fig. 9(b)-(e). It can be seen that the optimized device with $W_x = 1.5 \ \mu$m has the similar structure with that in the case of $W_x = 1.0 \ \mu$m.

(a)

(i) Initial structure

(ii) Structure in 1st step

(iii) Structure in 2nd step

(iv) Structure in 3rd step

(v) Optimized structure

(vi) Propagating field
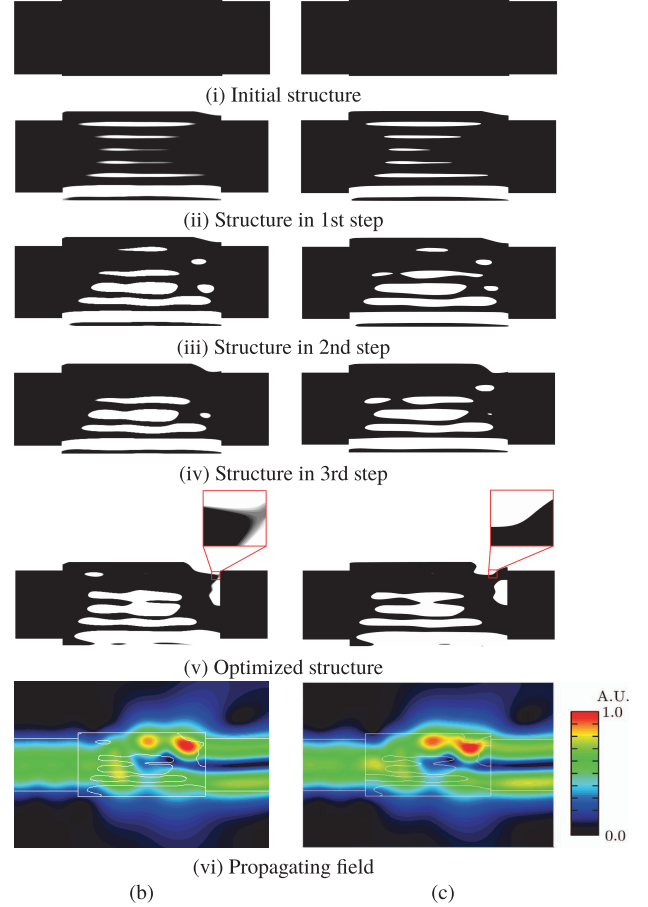
(b)   (c)

Fig. 8   Optimized results of mode converter. (a) The objective function and the normalized output power as a function of iteration count for topology optimization. The optimized structure and the propagating electric field obtained (b) with using gray area, (c) without using gray area. Initial structure, the structure in 1st, 2nd, and 3rd-steps, and the optimized structure are shown in order from the top.

Finally, we investigate the wavelength dependence of the mode order converters obtained by the present design approach. Figure 10 shows the wavelength dependence of the conversion efficiency and extinction ratio in the three optimized devices with $W_x = 0.5$, 1.0, and 1.5 μm. The conversion efficiency (CE) and the extinction ratio (ER) are
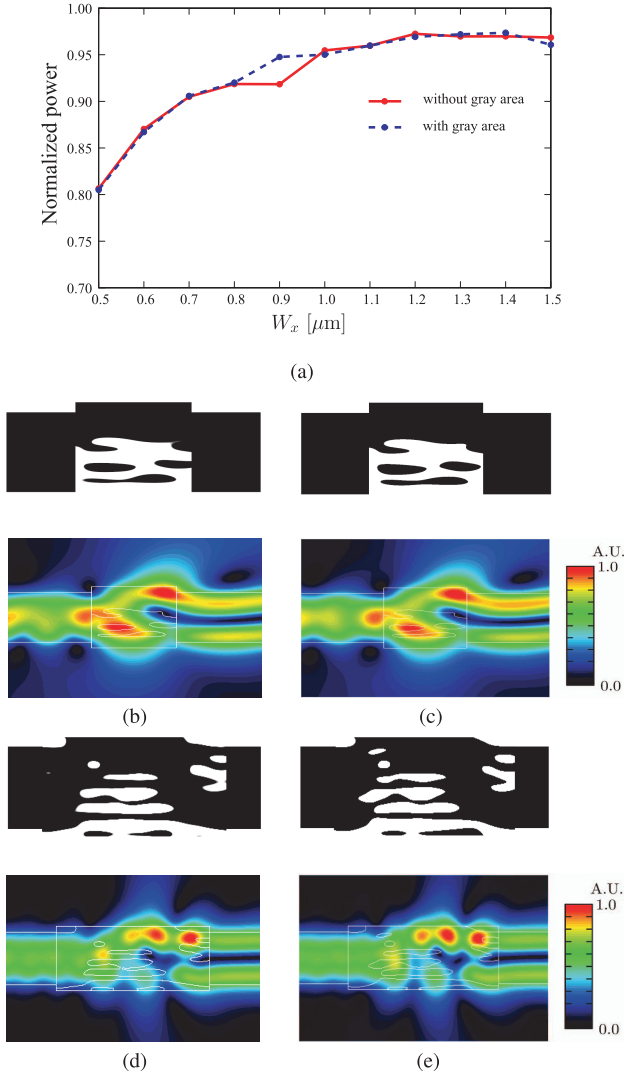
(a)

(b)   (c)

(d)   (e)

Fig. 9 Dependence of the optimized conversion efficiency on the design region size. (a) Conversion efficiency of optimized mode converters as a function of W_x. (b) and (c) are the optimized structures with device length of 0.5 μm and their propagating electric field. obtained by the conventional approach and present approach, respectively. (d) and (e) are the optimized structures with device length of 1.5 μm and their propagating electric field. obtained by the conventional approach and present approach, respectively.

defined as follows:

$$CE = \left| S_{21}^{TE_0 \to TE_1} \right|^2, \tag{19}$$

$$ER = 10 \log_{10} \frac{\left| S_{21}^{TE_0 \to TE_0} \right|^2}{\left| S_{21}^{TE_0 \to TE_1} \right|^2} \text{ [dB]}. \tag{20}$$

It can be seen that the optimized mode order converter has a relative small wavelength dependence and it has the ER of less than -20 dB over a wider bandwidth than 100 nm in the device with $W_x = 1.5$ μm and less than -18 dB in one with $W_x = 1.0$ μm. Although the optimized profile is sometimes relatively complicated in this design approach, there is a possibility that the optimized structure can be simplified by the scheme reported in [21].
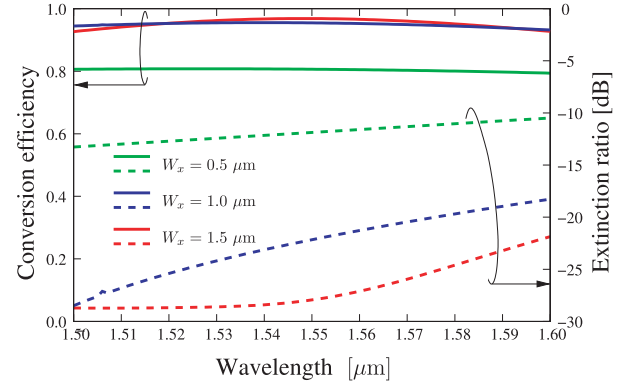

Fig. 10 Wavelength dependence of the optimized mode order converters with $W_x = 0.5,$ 1.0, and 1.5 μm.

4. Conclusion

We revised a sensitivity analysis method for function-expansion-based topology optimization method so as not to require gray area. Adaptive mesh generation process is also improved for accurate analysis. The validity of this approach is verified by comparing the results obtained by the present sensitivity method with those by the conventional one. In future work, we will design ultra compact photonic devices including plasmonic waveguide devices using the present optimization method. We studied on 2D topology optimization in this paper. In the conventional approach with gray area, we have been already developed 3D topology optimization [22], [23]. The proposed approach without gray area can be straightforwardly extended to 3D optimization. Furthermore, in the design of layered structure as treated in [23], the present approach may be superior for estimating the sensitivity with respect to layer thickness.

References

[1] S.J. Molesky, Z. Lin, A.Y. Piggott, W. Jin, J. Vučković, and A.W. Rodriguez, "Outlook for inverse design in nanophotonics," Nature Photon., vol.12, no.11, pp.659–670, Oct. 2018.

[2] J. Jiang, J. Cai, G.P. Nordin, and L. Li, "Parallel microgenetic algorithm design for photonic crystal and waveguide structures," Opt. Lett., vol.28, pp.2381–2383, Dec. 2003.

[3] L. Sanchis, A. Hakansson, D. Lopez-Zanon, J. Bravo-Avad, and J. Sanchez-Dehesa, "Integrated optical devices design by genetic algorithm," Appl. Phys. Lett., vol.84, pp.4460–4462, May 2004.

[4] Y. Sakamaki, T. Saida, T. Shibata, Y. Hida, T. Hashimoto, M. Tamura, and H. Takahashi, "Y-branch waveguides with stabilized splitting ratio designed by wavefront matching method," IEEE Photon. Technol. Lett., vol.18, no.7, pp.817–819, April 2006.

[5] J.S. Jensen and O. Sigmund, "Systematic design of photonic crystal structures using topology optimization: Low-loss waveguide bends," Phys. Lett., vol.84, no.12, pp.2022–2024, March 2004.

[6] J.S. Jensen, O. Sigmund, L.H. Frandsen, P.I. Borel, A. Harpoth, and M. Kristensen, "Topology design and fabrication of an efficient double 90/spl deg/ photonic Crystal waveguide bend," IEEE Photon. Technol. Lett., vol.17, no.6, pp.1202–1204, June 2005.

[7] Y. Tsuji, K. Hirayama, T. Nomura, K. Sato, and S. Nishiwaki, "Design of optical circuit devices based on topology optimization," IEEE Photon. Technol. Lett., vol.18, no.7, pp.850–852, April 2006.

[8]   W.R. Frei, D.A. Totorelli, and H.T. Johnson, "Geometry projection method for optimizing photonic nanostructures," Opt. Lett., vol.32, no.1, pp.88–97, Jan. 2008.

[9]   Y. Tsuji and K. Hirayama, "Design of optical circuit devices using topology optimization method with function-expansion-based refractive index distribution," IEEE Photon. Technol. Lett., vol.20, no.12, pp.982–984, June 2008.

[10] K. Fujimoto, Y. Tsuji, K. Hirayama, T. Yasui, S. Sato, and R. Kijima, "A study on topology optimization of optical circuits consisting of multi-materials," J. Lightw. Technol., vol.30, no.13, pp.2210–2215, July 2012.

[11] H. Goto, Y. Tsuji, T. Yasui, and K. Hirayama, "A study on optimization of waveguide dispersion property using function expansion based topology optimization method," IEICE Trans. Electron., vol.E97-C, no.7, pp.670–676, July 2014.

[12] Z. Zhang, Y. Tsuji, T. Yasui, and K. Hirayama, "Design of ultracompact triplexer with function-expansion based topology optimization," Opt. Exp. , vol.23, no.4, pp.3936–3950, Feb. 2015.

[13] A. Koda, K. Morimoto, and Y. Tsuji, "A study on topology optimization of plasmonic waveguide devices using function expansion method and evolutionary approach," J. Lightw. Technol., vol.37, no.3, pp.981–988, Feb. 2019.

[14] A. Koda, T. Tanaka, and Y. Tsuji, "A study on topology optimization of plasmonic waveguide device based on sensitivity analysis by adjoint variable method," IEICE Trans. Electron., vol.J102-C, no.5, pp.139–145, May 2019 (in Japanese).

[15] A.Y. Piggott, J. Lu, K.G. Lagoudakis, J. Petykiewicz, T.M. Babinec, and J. Vučković, "Inverse design and demonstration of a compact and broadband on-chip wavelength demultiplexer," Nature Photonics, vol.9, no.6, pp.374–377, May 2015.

[16] A.Y. Piggott, J. Petykiewicz, and J. Vučkovicć, "Fabrication-constrained nanophotonic inverse design," Scientific Reports, vol.7, #1786, May 2017.

[17] Z. Yu, H. Cui, and X. Sun, "Genetic-algorithm-optimized wideband on-chip polarization rotator with an ultrasmall footprint," Opt. Lett., vol.42, no.16, pp.3093–3096, Aug. 2017.

[18] A. Iguchi, Y. Tsuji, T. Yasui, and K. Hirayama, "Topology optimal design for optical waveguides using time domain beam propagation method," IEICE Electron. Express, vol.15, no.11, #20180417, May 2018.

[19] Y. Tsuji and M. Koshiba, "Finite element method using port truncation by perfectly matched layer boundary conditions for optical waveguide discontinuity problems," J. Lightw. Technol., vol.20, no.3, pp.463–468, March 2002.

[20] Y. Tsuji and M. Koshiba, "Simple and efficient adaptive mesh generation for approximate scalar guided-mode and beam-propagation solution," IEICE Trans. Electron., vol.E81-C, no.12, pp.1814–1820, Dec. 1998.

[21] A. Iguchi and Y. Tsuji, "Ultra-small shape-simplified optical diode derived from topology optimal design in plasmonic waveguide," IEICE Electron. Express, vol.16, no.22, 2019.

[22] T. Yasui, Y. Tsuji, J. Sugisaka, and K. Hirayama, "Design of three-dimensional optical circuit devices by using topology optimization method with function-expansion-based refractive index distribution," J. Lightw. Technol., vol.31, no.23, pp.3765–3770, Dec. 2013.

[23] S. Tomioka, T. Tanaka, K. Mori, and Y. Tsuji, "Design of polarization splitter and rotator using function-expansion based topology optimization considering two-layer structure," J. Adv. Simulation Sci. Eng., vol.6, no.1, pp.141–148, March 2019.

Masato Tomiyasu   received the B.S. degree in department of information and electrical engineering from Muroran Institute of technology, Muroran, Japan,in 2019. He is presently working toward the M.S, degree in Information and Electronic Engineering from Muroran Institute of Technology. Mr. Tomiyasu is a student member of the Institute of Electronics, Information and Communication Engineers (IEICE).
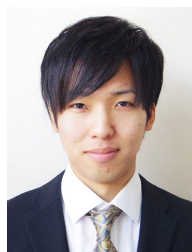
Keita Morimoto   received the B.S. and M.S. degrees in information and electronic engineering from the Muroran Institute of Technology, Muroran, Japan, in 2017 and 2019, respectively, where he is currently pursuing the Ph.D. degree in information and electronic engineering. Mr. Morimoto is a Student Member of the Institute of Electronics, Information and Communication Engineers (IEICE) and IEEE.

Akito Iguchi   received the B.S., M.S., and Ph.D. degrees in electronic engineering from Muroran Institute of Technology, Muroran, Japan, in 2015, 2017, and 2019. From 2019 to 2020, he was a Post-Doctoral Research Fellow of Japan Society for the Promotion of Science (JSPS). He is currently an Assistant Professor at Muroran Institute of Technology. Dr. Iguchi is a member of the Institute of Electronics, Information and Communication Engineers (IEICE) and IEEE.

Yasuhide Tsuji   received the B.S., M.S., and Ph.D. degrees in electronic engineering from Hokkaido University, Sapporo, Japan, in 1991, 1993, and 1996, respectively. In 1996, he joined the Department of Applied Electronic Engineering, Hokkaido Institute of Technology, Sapporo, Japan. From 1997 to 2004, he was an Associate Professor of Electronics and Information Engineering at Hokkaido University. From 2004 to 2011, he was an Associate Professor of Electrical and Electronic Engineering at Kitami Institute of Technology, Kitami, Japan. Since 2011, he has been a Professor of Information and Electronic Engineering at Muroran Institute of Technology, Muroran, Japan. He has been interested in wave electronics. Dr. Tsuji is a Senior Member of the Institute of Electronics, Information and Communication Engineers (IEICE), and the IEEE, and a Member of the Japan Society of Applied Physics and the Optical Society of America (OSA). In 1997, 1999, and 2019, he was awarded the Best Paper Award from IEICE. In 2000, he has received the Third Millennium Medal from IEEE. In 2019, he has received the IEEE Photonics Technology Letters Outstanding Reviewer Award.